Numerical Investigations of HSCT Inlet Unstart Transient at Angle of Attack

Ge-Cheng Zha*
CFD Research Section, Air Vehicle Directerate
Air Force Research Lab., Wright Patterson Air Force Base
Dayton, OH 45433-7913

Doyle Knight†
Dept. of Mechanical and Aerospace Engineering
Center for Computational Design
Rutgers University - The State University of New Jersey
98 Brett Road · Piscataway NJ 08854

Donald Smith‡
Dept. of Computer Sciences
Center for Computational Design
Rutgers University - The State University of New Jersey
Piscataway NJ 08854

Abstract

The unstart transient of a High Speed Civil Transport (HSCT) mixed compression axisymmetric inlet at Mach 2 and 2° angle of attack was investigated numerically by using a 3D time accurate Navier-Stokes solver. The Baldwin-Lomax algebraic turbulence model and an extrapolation uniform mass bleed boundary condition for the slot bleed were employed. It is observed that, when an angle of attack is imposed, the flow on the leeward side has a stronger compression than that at zero angle of attack. The strong compression reduces the Mach number upstream of the terminal shock and therefore makes the shock move upstream first on the leeward side. The initial shock motion starts with the bifurcation of the terminal shock. The lower part of the split shock is stable due to the centerbody bleed while the top part of the shock continues to travel upstream. When the terminal shock on the leeward side passes the bleed region, a separation is induced by the shock/boundary layer interaction on the shoulder of the inlet centerbody and the entire inlet is brought to unstart. The overall computed flow field phenomena agree qualitatively with the experimental observations.

* Visiting Scientist, AIAA Member
† Professor, AIAA Associate Fellow
‡ Research Associate Professor

1 Nomenclature

Symbol	Definition
M_∞	Free Stream Mach Number
$P_{t\infty}$	Free Stream Total Pressure
$T_{t\infty}$	Free Stream Total Temperature
Δx	grid point interval in axial direction
Δr	grid point interval in radial direction
Δr_1^+	$(\Delta r_1 u_\tau)/\nu$
δ	boundary layer thickness on center body
R_c	radius at cowl leading edge
t_c	characteristic time
α	angle of attack

2 Introduction

To meet the demands of efficiency and comfort of long distance inter-continental travel, second generation High Speed Civil Transports (HSCT)

are being developed and show an extremely promising market [1, 2]. Whereas the current generation of supersonic transports (Concorde and TU-144) employ external compression inlets, the next generation HSCT designs use the more efficient mixed compression type in which the terminal shock is located downstream of the cowl leading edge. Disturbances can cause the terminal shock to be expelled from the inlet ("inlet unstart") resulting in a loss of thrust. Therefore, prevention of inlet unstart is a critical issue to achieve a HSCT propulsion system with high efficiency and a wide stability margin.

The disturbance which can induce inlet unstart can be either a variation of flight conditions (i.e.: angle of attack, free stream Mach number, free stream pressure, etc.) or the corrected weight flow required by the compressor. To increase the inlet control operability, boundary layer bleed is usually employed in the region of the throat to control the disturbance. To study the mechanism of the inlet unstart in order to achieve good design of boundary layer bleed, wind tunnel tests are necessary. However, with current powerful computers, CFD can be used as a preliminary tool to analyze the transient phenomena of inlet unstart. Various numerical studies have been carried out focusing on inlet unstart transient due to different disturbances. Mayer and Paynter [3, 4] used an Euler solver and simulated an axisymmetric inlet unstart due to the variation of free stream variables such as temperature, velocity and pressure. Slater et al. [5, 6] simulated the unstart/restart due to the freestream disturbance with moving geometry. Neaves and McRae [7] used the dynamic solution-adaptive grid algorithm of Benson and McRae and simulated the 2D and 3D inlet unstart due to the freestream and compressor face perturbations. Goble et al. [8] used a 3D Euler code to simulate the unsteady flow of the F-22 inlet with the hammershock from the engine face. Miller and Smith conducted an Navier-Stokes simulation of 2D high speed inlet unstart due to the back pressure disturbance [9]. These studies made contributions from different aspects to investigate the high speed inlet unstart transient at zero angle of attack.

No numerical studies have been reported on high speed axisymmetric inlet unstart transient due to changes in the angle of attack. Zha et al. [10] accurately predicted the unstart angle of attack of a HSCT axisymmetric inlet with a 3D Navier-Stokes solver. Kawamura et al.[11] also simulated 3D axisymmetric HSCT inlet flow at angle of attack. However, the computations in these two studies were all for steady state flows.

Outside of the CFD work, it must be mentioned that Choby [12] was one of the earliest experimental investigators to study the mechanism of inlet unstart for a mixed compression axisymmetric inlet at angle of attack. He first observed the overcompression on the leeward side due to the angle of attack which caused the inlet unstart. However, due to the limited measurement data, the experiment did not give sufficient details of the whole flow field. In general, the cause of the axisymmetric inlet unstart due to the angle of attack has not been fully understood.

The purpose of the present work is to investigate the unstart transient mechanism of a typical axisymmetric HSCT inlet using CFD. Understanding of the physical phenomena of the unstart transient for axisymmetric HSCT inlet is very important to guide the HSCT inlet design and control to obtain high efficiency and wide stability margin [13]. The tolerance of angle of attack is a more challenging issue in the design of an axisymmetric HSCT inlet compared to a rectangular inlet. Resolving this issue will allow us to explore the inherent advantages of an axisymmetric HSCT inlet for its short length, light weight and high total pressure recovery. This work represents the first computational study of the axisymmetric HSCT inlet unstart mechanism due to angle of attack using a 3D time accurate Navier-Stokes solver.

3 The Inlet

The inlet studied in this work (Fig. 1) is the NASA Variable Diameter Centerbody (VDC) inlet designed and tested in Lewis Research Center [14, 15, 16]. It is a bicone, mixed-compression inlet with design cruise Mach number 2.5. A two-cone spike was used to provide the maximum external compression compatible with high total pressure recovery and relatively low cowl drag.

In order to vary the contraction ratio in flight, the angle of the second cone could vary, and at its lowest position it would blend into the first-cone contours so as to provide a single-cone centerbody. This structure provides 45% of the supersonic area contraction internally at a design Mach number of 2.5. The inlet was designed such that the isentropic compression from the cowl and the cowl-lip oblique shock were nearly focused at a single location on the inlet's centerbody. A centerbody bleed slot was provided over this compression region for boundary layer control just ahead of the inlet geometric throat. The inlet was tested at Mach numbers of 2.5 and 2. At Mach 2.5 and critical operation, the maximum total pressure recovery with only 0.02 centerbody bleed mass-flow ratio and no cowl bleed was 0.906. Critical operation is defined as operation with the terminal shock positioned at the inlet's geometry throat. The bleed mass-flow ratio is the ratio of bleed mass flow rate to the captured mass flow rate of the inlet. At Mach 2, the inlet total pressure recovery was 0.938 with only 0.013 centerbody bleed mass-flow ratio at critical operation. The experimental unstart angle of attack for the Mach 2 inlet is 1.3° at critical operation. In this study, we examine the Mach 2 case which had the downstream bypass door closed so that the computation can avoid computing the bypass flow. For the Mach 2 geometry, the initial cone angle was 12.5° and the second cone angle was 14.5°.

4 Numerical Procedures and Mesh

4.1 Flow Solver

The GASP code [17] was used as the CFD solver to compute the flow field. The Reynolds-averaged 3D compressible time dependent Navier-Stokes equations were solved. The Baldwin-Lomax algebraic turbulence model was used to simulate turbulence. This turbulence model works well to predict the steady state results for the inlet flows [10]. We continue to use this model here for its efficiency and fairly good accuracy performance. Since the Roe scheme failed in 3D flow due to an anomalous solution [18], the Van Leer upwind scheme was used in our computation to evaluate the inviscid fluxes. The other important merit of the Van Leer scheme was that the allowable CFL was about 5 times higher than that of the Roe scheme. This was particularly meaningful for this time accurate computation which is very CPU intensive. The third order MUCSL type differencing with Min-Mod limiter was used to evaluate the inviscid flux and central differencing was used for the viscous terms. The time marching method was first order accurate in the temporal direction with the hybrid AF/Relaxation algorithm[17].

4.2 Boundary Conditions

The upstream boundary condition (the front face in Fig. 2) used fixed variables equal to those of the freestream. The no-slip conditions were used for the centerbody and cowl walls. First order extrapolation was used for the outer boundary upstream of the cowl leading edge. This boundary condition worked well to avoid the wave reflection and therefore the computation of the outer zone of the inlet was omitted to save CPU time. At the subsonic outflow, the constant back pressure boundary condition was used and all other variables were first order extrapolated. The bleed boundary condition was first order extrapolation for all the variables except for the normal velocity which was determined based on uniform bleed mass flowrate[10]. This boundary condition, similar to the BC type 5 suggested by Chyu et at. [19], was proven to be a reasonable approximation to the slot bleed used in the experiment [10].

4.3 Mesh

The mesh size of 201x81x31 in streamwise, circumferential and radial direction respectively was used for the present computation for the NASA VDC inlet [14] as shown in Fig. 2. The narrow band before the inlet throat with dense mesh in the streamwise direction is the boundary layer bleed region. Table 1 and 2 show the flow conditions and mesh conditions respectively.

This mesh size was found to be necessary to

resolve the wall boundary layer and shock profile to obtain the accurate quantitative results for the steady state solutions [10]. Specifically, an axisymmetric grid refinement study was performed at zero angle of attack[10] using two different grids 201x81 and 401x161. The resultant flowfields were essentially identical (e.g., the back pressure for critical operation differed by only 0.17%). We therefore adopted the mesh size of 201x81 on the streamwise planes for the time accurate computation in the present study. The circumferential mesh size of 31 is considered as sufficient[10]. Certainly, the time accurate computation with this mesh size was CPU intensive. The whole computation took about 90 CPU days using a single processor of the SGI Origin2000 at ASC MSRC supercomputer center at Wright Patterson Air Force Base.

5 Results and Discussion

The steady state solution at zero angle of attack was computed using a variable time step and was used as the initial solution for the unsteady time accurate computation. The detailed procedure to compute the steady state solution is given in [10]. The angle of attack at the inflow plane was changed linearly in 10 equal increments from zero to 2° within $0.08t_c$, where t_c is the characteristic time defined as the time taken by a fluid particle to flow from the inlet entrance to the exit in the approximate speed along the centerline of the inlet duct. t_c is estimated to be about 6.25 milliseconds. Each increment of angle of attack took 125 time steps.

Fig. 3 is the computed wall pressure distributions of the steady state solutions compared with the experiment [14] along the centerbody at zero angle of attack and critical operation (pressure normalized by the freestream total pressure, length normalized by the cowl radius, R_c). It indicates that the computed shock location and intensity agree well with the experiment under the experimental back pressure. The experimental bleed mass rate of 1.3% was used. The computed pressure deviation in a portion of the subsonic diffuser is due to neglecting the four centerbody support struts installed in the experimental inlet from about x/R_c= 4.1 to x/R_C = 5.6 to simplify the problem. The centerbody struts make the cross-sectional area of the subsonic diffuser shrink and then expand, and therefore generate a pressure minimum in the experiment at x/Rc = 5.2 as shown in Fig. 3. The absence of the support struts has little influence of the shock position under the experimental back pressure [10], and therefore has little effect on the inlet unstart transient studied in this paper.

Fig. 4 presents the transient Mach number contours on the leeward and windward plane from the initial solution at zero angle of attack to the inlet unstart at 2° angle of attack. The time level of Fig. 4 a, b and c are at 0, $2.36t_c$ and $4.04t_c$ respectively. It is seen that the flow and the shock wave structure are axisymmetric at zero angle of attack (Fig. 4 a). By comparing the dotted line indicating the intersection of the oblique shock and the computational boundary in Fig. 4 a and b, it can be seen that when the 2° angle of attack is imposed, the centerbody oblique shock is non-axisymmetric and has higher shock angle on the leeward side and smaller shock angle on the windward side relative to the centerbody axis. This phenomenon agrees with the conical flow field analysis [20].

From Fig. 4 b, it is seen that, with angle of attack, the terminal shock on the leeward side moves upstream first. The windward side shock moves downstream slightly and is in a more stable position. When the leeward side terminal shock crosses the bleed region, it starts to cause separation on the shoulder of the centerbody. The separation region then rapidly spreads circumferentially and causes the entire inlet unstart as shown in Fig. 4 c. Fig. 4 c displays the shock system which is in the state just before it reaches the full unstart as shown in [10]. Fig. 4 c also indicates that the oblique shock from the leading edge of the centerbody is little influenced by the downstream shock motion due to the predominantly supersonic characteristics of the flow field in that portion.

At this point before we further analyze the computational results, we list the experimental observations by Choby [12] in order to compare with the computation. The experimental Mach

number and angle of attack were 2.5 and 2.7°, respectively. The experimental geometry was similar to our present one. The experimental results are summarized as the following:

1) The leeward side pressure field was strongly compressed, termed as overcompression by Choby, and caused the inlet to be choked upstream of the geometric throat. The maximum unstart angle was limited by the leeward side overcompression.
2) It was not clear how much of the inlet was encompassed by the region of overcompression since the pressure were measured only at two circumferential locations (windward and leeward plane).
3) The windward side had no overcompression and the pressure agreed well with the zero angle of attack case.
4) On the leeward side upstream of the cowl shock impingement, the boundary layer thickness was thicker at angle of attack than the one at zero angle of attack.

Since the flow conditions and inlet geometry of the experiment were different from those in our computation, we only seek qualitative comparison. Obviously, what we have presented agrees with the point 1 and 3 of Choby's experiment even though the inlet in the present computation is not choked.

Fig. 5 shows the leeward side terminal shock motion with time. Fig. 5 shows that on the leeward side, the initial significant move of the terminal shock occurs at about $0.9t_c$ and moves out of the bleed region at about $1.2t_c$. The fastest acoustic wave travels from the inlet entrance to the exit at the characteristic speed of $u+a$ and reflects back from the compressor face at the characteristic speed of $a-u$, where u is the main flow velocity and a is the speed of sound. It takes about $2.1t_c$ for the reflection of the fastest acoustic wave to arrive at the bleed region. This indicates that the initial terminal shock motion is not due to the acoustic wave reflection in this case since the shock has already moved a quite long distance when the reflection arrives as shown in Fig. 5. The windward side terminal shock has stayed in the bleed region until the leeward side terminal shock starts to generate the boundary layer separation on the shoulder of the centerbody and seriously block the inlet at about $2.36t_c$ (see Fig. 4 b). Fig. 5 also shows that it takes about 4 characteristic time for the inlet to fully unstart at 2^o angle of attack.

To analyze the cause for the leeward side initial terminal shock motion, it is useful to present the results at the time level when the leeward side terminal shock just starts to move.

Fig. 6 presents the Mach number contours and demonstrates the detailed initial terminal shock motion at time level of $0.79t_c, 0.88t_c$ and $1.01t_c$ in the region of the bleed. The terminal shock has remained as a single entity from the initial field to about $0.79t_c$ as shown in Fig. 6 a. The shock then gradually bifurcates into two parts at $0.88t_c$ (Fig. 6 b). The top part becomes a normal shock across the channel and continues to move upstream (Fig. 6 c). The lower part of the shock remains unmoved at the beginning and the shock intensity decreases. The lower part of the shock eventually disappears because the forward going normal shock becomes stronger and stronger and reduces the flow to subsonic after it. The centerbody bleed stabilizes the lower part of the shock, while the top part of the shock moves in the absence of cowl bleed.

The lower part of the bifurcated shock is also likely induced by the bleed process itself. According to Shih et al. [21], the bleed hole induces a so called " barrier shock" which is very similar to the lower part of the bifurcated shock. But the geometry and its scale in Shih's study were different. Their bleed hole had a thick non-dimensional wall and different diameter. In the present case, the downstream geometry of the bleed slot is a blunt lip wedge. In addition, the present flow field in the bleed region is simulated by bleed boundary condition instead of the real geometry. Therefore, without simulating the real bleed geometry, it is not fully clear whether the lower part of the shock is just a part of the terminal shock or the " barrier shock".

Fig. 7 shows the Mach number distributions at $0.88t_c$ (the same time level as Fig. 6 b) along the centerline between the centerbody and cowl wall on the leeward and windward plane compared with the case at zero angle of attack. This Mach number is approximately the highest Mach

number of the duct cross section and represents the capability of the duct section to pass mass flow. Upstream of the terminal shock, the Mach number at zero angle of attack is in the middle with the higher Mach number on the windward side and the lower Mach number on the leeward side at 2° angle of attack. It means that the flow on the windward side is less compressed and the flow on the leeward side is more compressed (overcompression [12]) compared with the case at zero angle of attack. The geometric throat is located at X/R_c =2.7836 and is downstream of the bleed region where the terminal shock stands. Fig. 7 indicates that the inlet is not choked at both 0° and 2° angle of attack since the peak centerline Mach number across the throat section on both the leeward and windward sides are clearly lower than 1.0.

Based on the above information provided by Fig. 7, we may come to the following explanation why the leeward side terminal shock moves upstream first.

We may use the 1D theory of unsteady moving shock in a shock tube [22] as an approximation to analyze the shock motion in the present flow field. According to [22], the shock motion Mach number relative to the inlet geometry is $M_s = M_1 - M_x$, where M_1 is the flow Mach number upstream of the normal terminal shock, M_x is shock propagation Mach number relative to the upstream flow and is expressed as $M_x = \sqrt{\frac{\gamma-1}{2\gamma}(1 + \frac{\gamma+1}{\gamma-1}\frac{p_2}{p_1})}$, where p is the pressure, subscript 1 represents the parameter upstream of the shock and 2 represents the parameter downstream of the shock. As we know, a shock being stabilized at a certain location means that $M_s = 0$ and $M_1 = M_x$. Since the terminal shock at zero angle of attack is stable, it means that the Mach number upstream of the terminal shock balances the terminal shock propagation Mach number M_x. Fig. 7 shows that the pressure ratios across the shock are about the same with and without angle of attack and therefore M_x is relatively little changed. When the angle of attack is imposed and the Mach number upstream of the terminal shock is reduced, the balance is lost. It yields $M_1 < M_x$, $M_s < 0$ and lets the terminal shock on the leeward side move upstream. The shock may be stabilized at a new location upstream where $M_1 = M_s$. Such location depends on the compression intensity of the upstream flow on the leeward side and therefore depends on the amount of the angle of attack imposed. If the angle of attack is very large, the shock therefore will continue to travel upstream until the inlet unstarts. On the contrary, the terminal shock on the windward side moves slightly downstream due to the higher Mach number upstream of the terminal shock as shown in Fig. 4 b. It is stabilized there until the leeward side terminal shock causes separation on the shoulder of the inlet centerbody and induces the whole inlet unstarted.

It is expected that the higher the free stream angle of attack, the stronger the flow is compressed on the leeward side, and therefore the faster the shock travels upstream. This is why the computational search of the minimum unstart angle is extremely CPU intensive since the shock moves very slowly when it is approaching the minimum unstart angle. It therefore needs to run very long time to achieve the steady state solution. Usually an uncertainty range needs to be accepted to avoid the lengthy computation [10].

Fig. 8 is the wall pressure distributions on the leeward and windward planes at time level $0.88t_c$. On most part of the forward centerbody from the leading edge to $x/R_c \approx 1.4$, the circumferential pressure gradient direction on the wall is from leeward side to windward side. This also agrees with the conical flow at angle of attack [20]. However, the pressure gradient on the wall reverses the direction when it is close to the cowl leading edge (cowl leading edge is located at X/R_c = 2.0) with the flow compressed more strongly on the leeward side. This is again the so called overcompression observed by Choby [12] in his experiment.

Above phenomenon can also be seen from Fig. 9 which presents the pressure contours in circumferential direction at two streamwise locations at time level $0.88t_c$. Fig. 9 shows that the pressure gradient close to the centerbody wall at X/R_c = 1.22 is from leeward side to windward side and is reversed when it is close to the cowl leading edge at $x/R_c = 1.87$. Fig. 9 b also answers the point 2 of Choby's experiment that most of the leeward part of the inlet was encom-

passed by the region of the overcompression.

Fig. 10 presents the boundary layer displacement thickness development on the symmetric leeward and windward plane at 0° and 2° angle of attack upstream of the cowl shock impingement. The boundary layer thickness is measured based on the total pressure criterion as used in the experiment. The 2° case is at time level of $0.88t_c$. The leeward side boundary layer displacement thickness on the centerbody is thicker than the one at zero angle of attack. At angle of attack, the boundary layer on the windward side is thinner than the one on leeward side and also the one at zero angle of attack. This agrees with Choby's experimental observation point 4. The boundary layer on the leeward side may be thickened first by the migration of the boundary layer expelled by the pressure gradient from windward to leeward side. It is then further thickened by the stronger adverse pressure gradient due to the overcompression on the leeward side when it is close and inside the cowl.

There are at least three criteria which can be used to compute the boundary layer thickness for Fig. 10. They can be the following parameters at center line across the local duct section: total pressure, velocity, product of velocity and density. Based on the examination of the flow field computed, we have the following observations: Because the local velocity profile is not as regular as that of the flat plate, the centerline velocity is a very poor criterion to measure the boundary layer thickness and was not used in this computation. The product of velocity and density is a better criterion even though it yields unrealistic results upstream of the bleed region. The total pressure is the best criterion and has similar results to those using the product of velocity and density in most of the region. The uncertainty for Fig. 10 by using total pressure or density-velocity product to measure the boundary layer thickness is about 6%. Nonetheless, both criteria give the same trend and therefore the conclusion for Fig. 10 is the same.

6 Conclusions

The unstart transient of a High Speed Civil Transport (HSCT) axisymmetric inlet at Mach 2 and 2° angle of attack was investigated numerically by using a 3D time accurate Navier-Stokes solver. The Baldwin-Lomax algebraic turbulence model and an extrapolation uniform mass bleed boundary condition for the slot bleed were employed. It is observed that, when an angle of attack is imposed, the flow on the leeward side near the cowl leading edge has a stronger compression than that at zero angle of attack. The strong compression reduces the flow Mach number upstream of the terminal shock and therefore makes the shock move upstream first on the leeward side. The initial shock motion starts with the bifurcation of the terminal shock on the leeward side. The lower part of the shock is stable at the beginning due to the centerbody bleed while the top part of the shock continues to travel upstream. The lower part of the shock eventually disappears because the forward going normal shock becomes stronger and stronger and reduces the flow to subsonic after it. When the terminal shock on the leeward side crosses the bleed region, flow separation is induced on the shoulder of the inlet centerbody by the shock/boundary layer interaction. The separation first occurs on the leeward side and then rapidly spreads to the whole inlet and results in the entire inlet unstart. The acoustic wave reflection from the compressor surface is not the factor to expel the terminal shock in the case studied in this paper. The shock wave structure on the windward plane remains stable until the separation on the centerbody shoulder caused by the leeward side shock occurs. In the portion upstream of the cowl shock impingement on the centerbody, the boundary layer on the leeward side at angle of attack is thicker than the one on the windward side and also thicker than the one at zero angle of attack.

The overall computed flow field phenomena agree qualitatively with the experimental observations. Furthermore, the present computation provides more data than the experiment to understand the whole structure and mechanism of the inlet unstart.

7 Acknowledgments

This research is part of the HPCD (Hypercomputing and Design) project based at Rutgers University. The HPCD project is supported by the Defense Advanced Research Projects Agency of the Department of Defense through contract ARPA-DABT 63-93-C-0064 monitored by Dr. Bob Lucas. The contents of this paper do not necessarily reflect the position of the United States government and official endorsement should not be inferred. The computation work was conducted in ASC MSRC Supercomputer Center at Wright Patterson Air Force Base. The authors greatly appreciate Mr. Marty Haas, senior research engineer at UTRC, for his direction and suggestions for this work. We would also like to thank Mr. John D. Saunders at NASA Lewis Research Center and Dr. Gerald C. Paynter at Boeing for their helpful discussions.

References

[1] National Research Council, *Aeronautical Technologies for the Twenty-First Century.* Committee on Aeronautical Technologies, National Research Council, National Academy Press, Washington, D.C., 1992.

[2] National Science and Technology Council, *Goals for a National Partnership in Aeronautics Research and Technology.* Executive Office of the President of the United States, White House, 1995.

[3] D. Mayer and G. C. Paynter, "Prediction of Supersonic Inlet Unstart Caused by Freestream Disturbances," *AIAA Journal*, vol. 33, pp. 266–275, Feb. 1995.

[4] D. Mayer and G. C. Paynter, "Boundary Conditions for Unsteady Supersonic Inlet Analyses," *AIAA Journal*, vol. 32, pp. 1200–1206, June, 1994.

[5] J. W. Slater, "Efficient Computation of Unsteady Planar Internal Viscous Flows with Moving Geometry." AIAA Paper 96-0113, 1996.

[6] J. W. Slater, J. Chung, and G. L. Cole, "Computation of Unsteady Aeropropulsion Flows with Moving Geometry." Proceedings of 1st AFOSR Conference on Dynamic Motion CFD, Rutgers University, New Jersey, USA, June 3-5, 1996.

[7] M. D. Neaves and D. S. McRae, "Numerical Investigations of Axisymmetric and Three-Dimensional Supersonic Inlet Flow Dynamics Using a Solution Adaptive Mesh." Proceedings of 1st AFOSR Conference on Dynamic Motion CFD, Rutgers University, New Jersey, USA, June 3-5, 1996.

[8] B. D. Goble, S. King, J. Terry, and M. Schoop, "Inlet Hammershock Analysis Using a 3-D Unsteady Euler/Navier-Stokes Code." AIAA Paper 96-2547, 1996.

[9] D. N. Miller and B. R. Smith, "Time-Dependent CFD Analysis of Inlet Unstart." Proceedings of 1st AFOSR Conference on Dynamic Motion CFD, Rutgers University, New Jersey, USA, June 3-5, 1996.

[10] G.-C. Zha, D. Knight, D. Smith, and M. Haas, "Numerical Simulation of High Speed Civil Transport Inlet Operability with Angle of Attack," *AIAA Journal*, vol. 36, No. 7, pp. 1223–1229, 1998.

[11] T. Kawamura, W. Chyu, and D. Bencze, "Numerical Simulation of Three-Dimensional Supersonic Inlet Flow Fields." AIAA 87-0160, 1987.

[12] D. A. Choby, "Tolerance of Mach 2.50 Axisymmetric Mixed-Compression Inlet to Upstream Flow Variations." NASA TM X-2433, 1972.

[13] D. N. Bowditch, "Some Design Considerations for Supersonic Cruise Mixed Compression Inlets." NASA TM X-71460, 1973.

[14] J. F. Wasserbauer, R. J. Shaw, and H. E. Neumann, "Design of a Very-Low-Bleed Mach 2.5 Mixed-Compression Inlet with 45 Percent Internal Contraction." NASA TM X-3135, 1975.

[15] J. F. Wasserbauer, H. E. Neumann, and R. J. Shaw, "Distortion in a Full-Scale Bicone Inlet with Internal Focused Compression and 45 Percent Internal Contraction." NASA TM X-3133, 1974.

[16] J. F. Wasserbauer, H. E. Neumann, and R. J. Shaw, "Performance and Surge Limits of a TF30-P-3 Turbofan Engine/Axisymmetric Mixed-Compressino Inlet Propulsion Syetem at Mach 2.5." NASA TP 2461, 1985.

[17] "GASP v3 User's Manual." Aerosoft, Inc., May 1996.

[18] G.-C. Zha, D. Knight, D. Smith, and M. Haas, "Numerical Simulation of HSCT Inlet Operability with the Angle of Attack." AIAA 97-2761, 1997.

[19] W. Chyu, G. Howe, and T. I.-P. Shih, "Bleed Boundary Conditions for Numerically Simulated Mixed-Compression Sipersonic Inlet Flow," *Journal of Propulsion and Power*, vol. 8, pp. 862–868, July-Aug. 1992.

[20] John D. Anderson, Jr., *Modern Compressible Flow, Second Edition.* McGraw-Hill Publishing Company, 1990.

[21] T. I.-P. Shih, M. Rimlinger, and W. Chyu, "Three-Dimensional Shock-Wave/Boundary-Layer Interactions with Bleed," *AIAA Journal*, vol. 31, No. 10, pp. 1819–1826, Oct. 1993.

[22] Ascher H. Shapiro, *The Dynamics and Thermodynamics of Compressible Fluid Flow.* John Wiley & Sons, Inc., 1953.

[23] G.-C. Zha, D. Knight, and D. Smith, "Numerical Investigations of HSCT Inlet Uustart Transient at Angle of Attack." AIAA 98-3583, 1998.

Table 1: Flow Conditions

Parameter	*Value*
M_∞	2.0
angle of attack	2.0°
$P_{t\infty}$	7.67×10^4 Pa
$T_{t\infty}$	$390^0 K$
Reynolds No.	6.54×10^6 /m
bleed mass/captured mass	1.3%

Table 2: Grid Parameters

Parameters	*Quantity*
grid points in streamwise	201
grid points in radial	81
grid points in circumferential	31
$\Delta x/\delta_{throat}$	0.3
$\Delta r^+_{1\,max,centerbody}$	2.3
$\Delta r^+_{1\,ave,centerbody}$	1.3
$\Delta r^+_{1\,max,cowl}$	1.9
$\Delta r^+_{1\,ave,cowl}$	1.1
grid points within both BL_{throat}	33
grid cells within bleed region	12

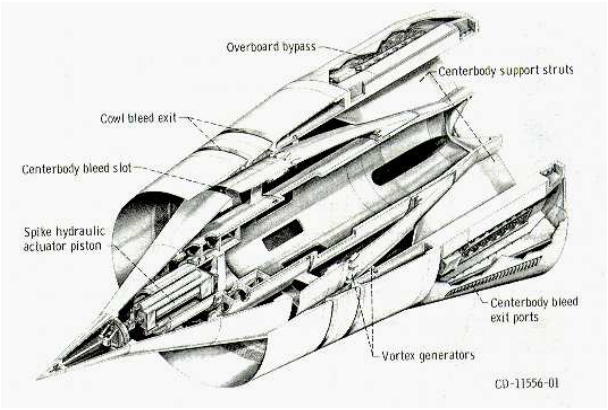

Figure 1: NASA VDC inlet cross section (from [14])

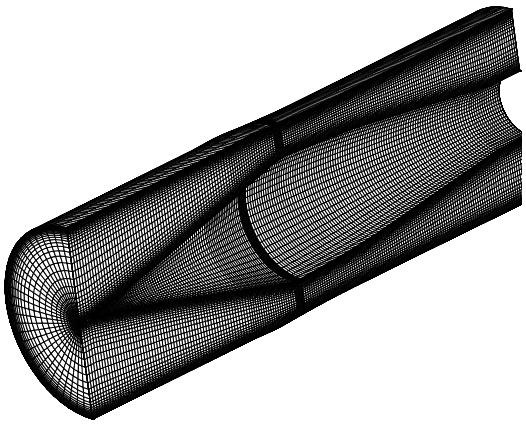

Figure 2: Geometry and mesh of the mixed compression inlet

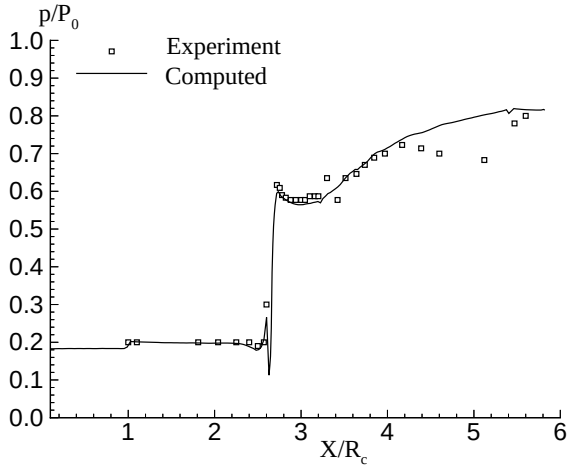

Figure 3: Wall pressure distributions along the centerbody of the inlet for M=2.0 at $\alpha = 0°$

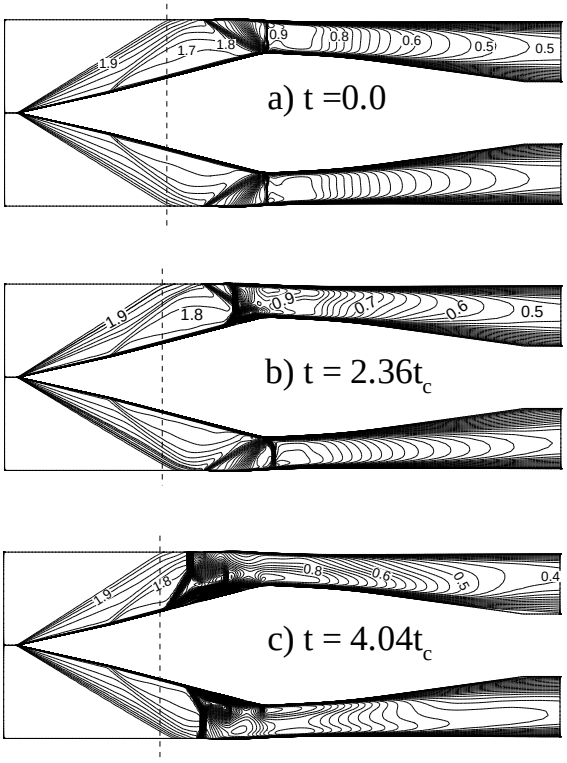

Figure 4: Mach number contours from zero angle of attack to inlet unstart 2° angle of attack, a) zero angle of attack, t=0; b) 2° angle of attack, t= $2.36t_c$; c) 2° angle of attack, t= $4.04t_c$;

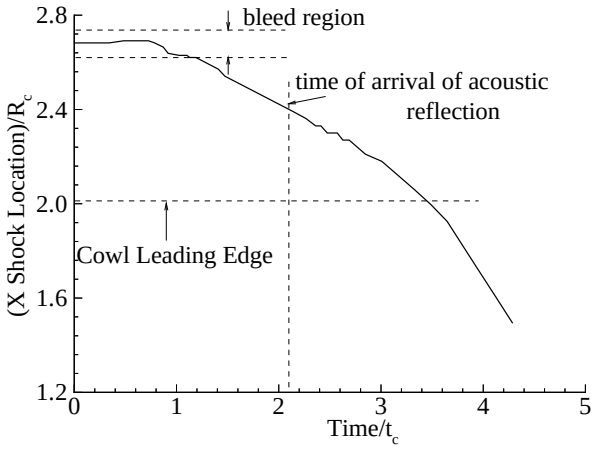

Figure 5: Leeward side terminal shock motion with time

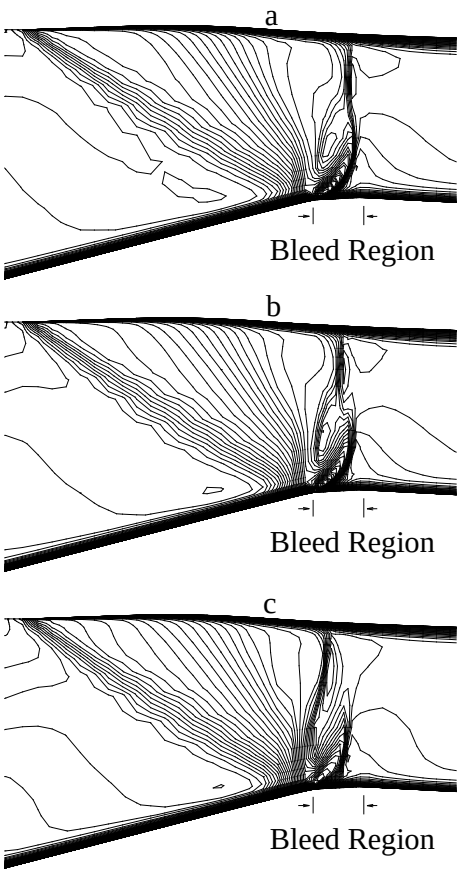

Figure 6: Mach number contours showing the initial shock motion on the leeward plane in the region of bleed, a) time level $0.79t_c$, b) time level $0.88t_c$, c) time level $1.01t_c$

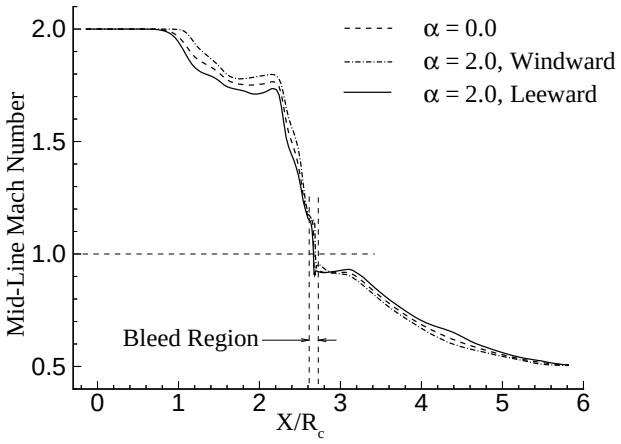

Figure 7: Mach number distributions along the channel centerline on the leeward and windward plane at time level $0.88t_c$

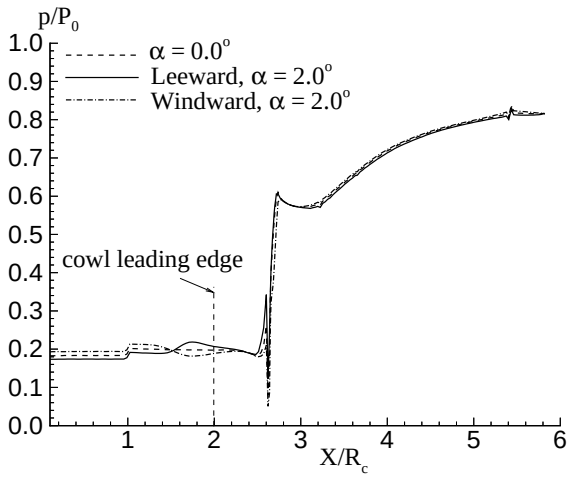

Figure 8: Wall pressure distributions on the leeward and windward plane at time level $0.88t_c$

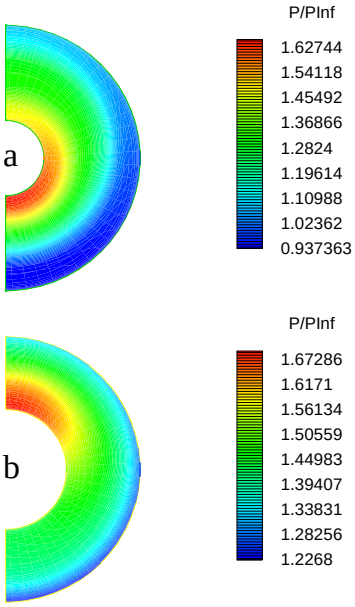

Figure 9: Spanwise pressure contours in the forward portion of the inlet at time level $0.88t_c$, a) $X/R_C = 1.22$, b) $X/R_C = 1.87$

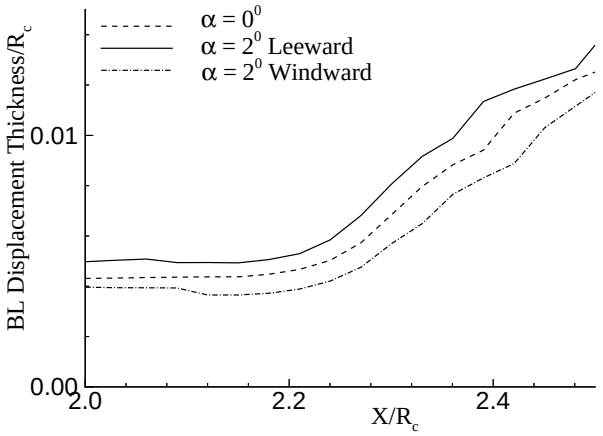

Figure 10: Centerbody boundary layer displacement thickness on the leeward and windward plane at time level $0.88t_c$